PTEP

Prog. Theor. Exp. Phys. **2023** 013H01(21 pages)
DOI: 10.1093/ptep/ptac170

Development of ultra-pure gadolinium sulfate for the Super-Kamiokande gadolinium project

K. Hosokawa[1], M. Ikeda[1,⋆], T. Okada[1], H. Sekiya[1,2], P. Fernández[3,†], L. Labarga[3], I. Bandac[4], J. Perez[4,‡], S. Ito[5], M. Harada[6], Y. Koshio[2,6], M. D. Thiesse[7], L. F. Thompson[7], P. R. Scovell[8], E. Meehan[8], K. Ichimura[9], Y. Kishimoto[9], Y. Nakajima[10], M. R. Vagins[2,11], H. Ito[12], Y. Takaku[13], Y. Tanaka[14], and Y. Yamaguchi[14]

[1]*Kamioka Observatory, Institute for Cosmic Ray Research, University of Tokyo, Kamioka, Gifu 506-1205, Japan*
[2]*Kavli Institute for the Physics and Mathematics of the Universe (WPI), The University of Tokyo Institutes for Advanced Study, University of Tokyo, Kashiwa, Chiba 277-8583, Japan*
[3]*Department of Theoretical Physics, University Autonoma Madrid, Madrid, 28049, Spain*
[4]*Laboratorio Subterraneo de Canfranc, Canfranc Estacion, Huesca, 22880, Spain*
[5]*High Energy Accelerator Research Organization (KEK), Tsukuba, Ibaraki 305-0801, Japan*
[6]*Department of Physics, Okayama University, Okayama, Okayama 700-8530, Japan*
[7]*Department of Physics and Astronomy, The University of Sheffield, Sheffield S3 7RH, UK*
[8]*Boulby Underground Laboratory, Saltburn-by-the-Sea, Redcar & Cleveland TS13 4UZ, UK*
[9]*Tohoku University Research Center for Neutrino Science, Sendai, Miyagi 980-8578, Japan*
[10]*Department of Physics, University of Tokyo, Bunkyo, Tokyo 113-0033, Japan*
[11]*Department of Physics and Astronomy, University of California, Irvine, Irvine, CA 92697-4575, USA*
[12]*Department of Physics, Faculty of Science and Technology, Tokyo University of Science, Noda, Chiba 278-8510, Japan*
[13]*Faculty of Pure and Applied Science, University of Tsukuba, Tsukuba, Ibaraki 305-8577, Japan*
[14]*Nippon Yttrium Co., Ltd., Omuta, Fukuoka 836-0003, Japan*

⋆E-mail: motoyasu@suketto.icrr.u-tokyo.ac.jp
[†]Currently at Donostia International Physics Center DIPC, San Sebastián/Donostia, E-20018, Spain
[‡]Currently at M. Smoluchowski Institute of Physics, Jagiellonian University, 30-348 Kraków, Poland

Received September 13, 2022; Revised November 30, 2022; Accepted December 9, 2022; Published December 12, 2022

This paper reports the development and detailed properties of about 13 metric tons of gadolinium sulfate octahydrate, $Gd_2(SO_4)_3 \cdot 8H_2O$, which has been dissolved into Super-Kamiokande (SK) in the summer of 2020. We evaluate the impact of radioactive impurities in $Gd_2(SO_4)_3 \cdot 8H_2O$ on diffuse supernova neutrino background searches and solar neutrino observation and confirm the need to reduce radioactive and fluorescent impurities by about three orders of magnitude from commercially available high-purity $Gd_2(SO_4)_3 \cdot 8H_2O$. In order to produce ultra-high-purity $Gd_2(SO_4)_3 \cdot 8H_2O$, we have developed a method to remove impurities from gadolinium oxide, Gd_2O_3, consisting of acid dissolution, solvent extraction, and pH control processes, followed by a high-purity sulfation process. All of the produced ultra-high-purity $Gd_2(SO_4)_3 \cdot 8H_2O$ is assayed by inductively coupled plasma mass spectrometry and high-purity germanium detectors to evaluate its quality. Because of the long measurement time of high-purity germanium detectors, we have employed several underground laboratories for making parallel measurements including the Laboratorio Subterráneo de Canfranc in Spain, Boulby in the UK, and Kamioka in Japan. In the first half of production, the measured batch purities were found to be con-

sistent with the specifications. However, in the latter half, the $Gd_2(SO_4)_3 \cdot 8H_2O$ contained one order of magnitude more ^{228}Ra than the budgeted mean contamination. This was correlated with the corresponding characteristics of the raw material Gd_2O_3, in which an intrinsically large contamination was present. Based on their modest impact on SK physics, they were nevertheless introduced into the detector. To reduce ^{228}Ra for the next stage of gadolinium loading to SK, a new process has been successfully established.

Subject Index H20, H51

1. Introduction

Super-Kamiokande (SK) [1] is a 50-kton water Cherenkov detector located in Hida-city, Japan and has been operational since 1996. The experiment started with pure water as the detection medium and has made world-leading measurements of astrophysical, atmospheric, and accelerator neutrinos, as well as searches for nucleon decays. To further enhance its physics capability, such as searching for the diffuse supernova neutrino background (DSNB), it was proposed to add gadolinium to the SK detector (SK-Gd) [2]. Gadolinium, in the form of $Gd_2(SO_4)_3 \cdot 8H_2O$, is expected to significantly enhance the neutron detection capability of SK due to its large thermal neutron capture cross section and subsequent ∼8-MeV γ-ray emission.

While one of the primary physics goals of SK-Gd is to detect the DSNB signal via inverse-β reactions ($\bar{\nu}_e + p \rightarrow e^+ + n$), measurements of conventional physics targets will continue with similar sensitivities as before. One challenge to overcome in the realization of the SK-Gd project is to mass-produce many metric tons of $Gd_2(SO_4)_3 \cdot 8H_2O$ with impurities low enough so that, when dissolved into SK, backgrounds for the solar neutrino analysis at SK would not increase significantly and the detector performance would not be otherwise adversely affected. To achieve this, we developed a scalable purification method and conducted highly sensitive radiopurity assays at multiple sites. These efforts were critical for the successful first gadolinium loading of the SK detector in 2020 [3].

This paper summarizes the purification method and the purity screening for 13 metric tons of high-purity $Gd_2(SO_4)_3 \cdot 8H_2O$ used in the first gadolinium loading of SK in 2020. The first loading resulted in a gadolinium concentration of 0.011%, corresponding to a neutron capture efficiency of about 50%. In 2022, following the success of the first introduction, we loaded 26 metric tons of $Gd_2(SO_4)_3 \cdot 8H_2O$ and achieved a gadolinium concentration of 0.033% (neutron capture efficiency of approximately 75%). For the second loading, we had developed an additional purification process to produce even cleaner powder than that of the first loading as discussed in Sect. 7. The final goal of SK-Gd is to achieve a gadolinium concentration of 0.1% (neutron capture efficiency of around 90%) and future plans will be determined based on the current concentration observations. The expected the duration of the SK-Gd phase is of the order of ten years.

In this paper, we first present and justify the requirements imposed on radioactive impurities in the $Gd_2(SO_4)_3 \cdot 8H_2O$ in Sect. 2. Section 3 describes the level of typical impurities of commercially available $Gd_2(SO_4)_3 \cdot 8H_2O$, which motivated significant R&D of the purification methods described in Sect. 4. We describe the low-background, low-activity radioimpurity assay methods in Sect. 5 and their results in Sect. 6. Finally, we describe further improved purification methods, which will be employed for future gadolinium loading, in Sect. 7.

2. Requirements

While the addition of gadolinium to SK will allow more efficient neutron tagging, any impurities present in the raw $Gd_2(SO_4)_3 \cdot 8H_2O$ would also be present in the detection medium. Radioactive impurities may contribute to the low-energy backgrounds and affect the sensitivity of SK-Gd to the observation of the DSNB and solar neutrino measurements (4–20 MeV). To maintain these sensitivities, stringent requirements are set on the radioactive purity of the $Gd_2(SO_4)_3 \cdot 8H_2O$ material to be introduced into SK.

In Sect. 2.1, we consider γ emission accompanied by a neutron from radioactive contaminants; these neutrons are produced throughout the detector and their detection could mimic an antineutrino inverse-β decay (IBD) signal.

Further, in Sects. 2.2 and 2.3, the relevant radioactive impurities to be controlled include those that emit γ or β radiation with sufficient energy to mimic signals from low-energy, $\mathcal{O}$(MeV), neutrino interactions.

In this section, we study the radioactivity-induced backgrounds for SK-Gd and set the requirements on the $Gd_2(SO_4)_3 \cdot 8H_2O$ impurities based on the physics analyses they impact. We also justify the limit imposed on the fluorescent cerium concentration to prevent a significant adverse change in detector performance. In the text, the radioactive decay chains are separated into their early (E) and late (L) sub-chains. Where appropriate, these sub-chains are referred to by their longest-lived isotopes.

For all these studies we assume 0.2% concentration of $Gd_2(SO_4)_3 \cdot 8H_2O$, or 0.1% concentration of gadolinium. We also assume that the nuclides in each sub-chain are all in secular equilibrium, but the sub-chains in each decay chain (i.e. ^{238}U, ^{232}Th, ^{235}U) are not necessarily in secular equilibrium due to the significant chemical processing taken place during the purification.

2.1 *^{238}U spontaneous fission*

A small fraction of ^{238}U decays are the result of spontaneous fission (SF), as are even smaller fractions of ^{235}U and ^{232}Th due to their lower masses. A neutron captured on gadolinium and the resulting γ cascade following an SF event can be indistinguishable from an antineutrino IBD if only one γ and one neutron are detected. Therefore, these decays represent an irreducible source of background for measuring low-energy antineutrinos from the DSNB, nuclear reactors, and the silicon-burning phase prior to a supernova burst.

The number of ^{238}U decays which fake an antineutrino IBD is calculated using several factors. First, the likelihood of ^{238}U to decay by SF is 5.4×10^{-7} [4]. Second, the target concentration of $Gd_2(SO_4)_3 \cdot 8H_2O$ in SK-Gd is 0.2%. And third, the number of high-energy, $\mathcal{O}$(MeV), photons produced with energy $E_{\rm min} \leq E_\gamma \leq E_{\rm max}$ in an SF decay, as derived from the emission spectrum measured in [5], is:

$$N^{\gamma}_{\rm SF}(E_{\rm min}, E_{\rm max}) = 0.99 \times \left(e^{-\frac{E_{\rm min}}{1.41}} - e^{-\frac{E_{\rm max}}{1.41}} \right), \quad (1)$$

where the factors 0.99 and 1.41 are the normalization and slope of the exponential fit to the data in Ref. [4] of γ-emission rate from ^{238}U SF as a function of the energy. One should also note that in SK, photons are reconstructed as electrons with 0.511 MeV less energy due to the electron mass.

For an SF decay to mimic an antineutrino IBD, one emitted neutron must be detected. Combining the neutron multiplicity probability [6,7] from ^{238}U SF with the SK estimated neutron

tagging efficiency of 80% (given the 0.2% concentration of $Gd_2(SO_4)_3 \cdot 8H_2O$) along with calculations in Ref. [8], the irreducible background rate (events per second) for antineutrino IBD events from ^{238}U SF is

$$R_{^{238}\mathrm{U-SF}}(1\gamma + 1\mathrm{n}) = \left(5.4 \times 10^{-7}\right) \times 0.364 \times \mathcal{C}_{^{238}\mathrm{U}} \times 0.2\% \times m_{\mathrm{FV}} \times N^{\gamma}_{\mathrm{SF}}(E_{\mathrm{min}}, E_{\mathrm{max}}), \quad (2)$$

where 5.4×10^{-7} is the ^{238}U SF rate per decay, m_{FV} is the mass of the SK fiducial volume (around 22.5×10^6 kg depending on the physics analysis), $\mathcal{C}_{^{238}\mathrm{U}}$ is the specific activity of ^{238}U in the $Gd_2(SO_4)_3 \cdot 8H_2O$ in units of Bq/kg and 0.2% is the target $Gd_2(SO_4)_3 \cdot 8H_2O$ concentration in SK-Gd. The factor 0.364 is the fraction of ^{238}U SF decays with a single reconstructed neutron. This accounts for the neutron multiplicity distribution measured in Ref. [6] and the above 80% neutron tagging efficiency, which depends on the target $Gd_2(SO_4)_3 \cdot 8H_2O$ concentration.

For the SK DSNB analysis, events with reconstructed energy from 10 to 20 MeV are considered. For reactor neutrinos, the photon energies relevant are from 3 to 10 MeV, where the minimum energy is limited by the SK low-energy threshold.

The irreducible backgrounds from ^{238}U SF which mimic antineutrino IBD events impact the reactor antineutrino detection analysis, the DSNB measurement, and the detection of pre-supernova antineutrinos at SK. Among these analyses, the detection of the DSNB is most constrained by backgrounds from ^{238}U SF [8].

Depending on the theoretical model for the DSNB, the expected signal rate at SK ranges from 0.6 to 5.3 events per year with antineutrino energy above 10 MeV [9]. To maintain a favourable signal-to-background ratio, the concentration of ^{238}U in dissolved $Gd_2(SO_4)_3 \cdot 8H_2O$ is limited to less than 5 mBq/kg, which corresponds to about 0.8 events per year in the SK fiducial volume from Eq. (2).

2.2 *β rays from radioactivity*

Sources of β radiation in SK primarily impact the solar neutrino analysis because those βs mimic low-energy electron neutrino interactions. Additionally, a β decay when coincident with a neutrino interaction may mimic an antineutrino IBD event. The most significant β-decay backgrounds are those that come from decays with a large branching fraction in the respective decay chain and a high Q-value: ^{208}Tl ($Q_\beta = 5.00$ MeV, 35.9% of ^{228}Th decays), ^{212}Bi ($Q_\beta = 2.25$ MeV, 64.1% of ^{228}Th decays), and ^{214}Bi ($Q_\beta = 3.27$ MeV, nearly 100% of ^{226}Ra decays). These βs may be reconstructed as the signal of low-energy neutrinos for the lowest energy bins in the SK solar neutrino analysis. According to Ref. [8], the fraction of these β decays which pass the SK solar neutrino cuts are 0.19% for ^{208}Tl, 0.01% for ^{214}Bi, and $<2 \times 10^{-4}$% for ^{212}Bi.

The expected total event rate in SK is around 200 per day after the event selections with recoil electron kinetic energy between 3.5 and 10 MeV in the solar neutrino analysis [10]. From the above estimates, 0.05 mBq/kg of ^{208}Tl contamination will produce about 130 solar neutrino candidate background events per day. About 190 candidate background events is expected from the β decay of ^{214}Bi in the late part of the ^{238}U chain (^{226}Ra equilibrium) for a 0.5-mBq/kg contamination.

2.3 *Radioactivity-induced neutron production*

^{238}U SF is the main neutron producer in the SK fiducial volume. For these decays, 67% of the final states contain more than one neutron [6], making these background events easily dis-

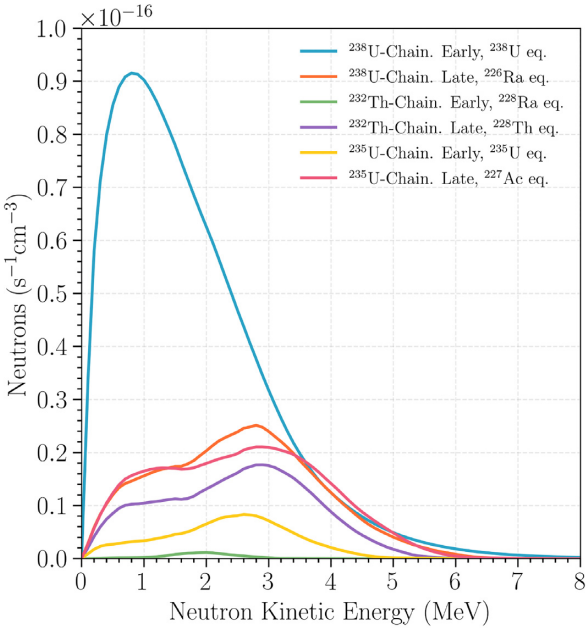

Fig. 1. The neutron production spectrum from each part, early and late, of the ^{238}U, ^{232}Th, and ^{235}U chains assuming secular equilibrium, an activity of 1 mBq/kg each, and 0.2% $Gd_2(SO_4)_3 \cdot 8H_2O$.

tinguishable from solar neutrino candidates considering the high neutron tagging efficiency in SK-Gd.

However, (α, n) reactions on oxygen from all α decays in all radioactive chains comprise another irreducible source of background for solar neutrino candidate events in SK as the emitted neutrons are captured by gadolinium, producing an 8 MeV γ cascade. In fact, 40% of neutron captures on gadolinium pass the SK solar neutrino cuts [8].

As ^{18}O is naturally five times more abundant than ^{17}O, these reactions occur mostly on ^{18}O nuclei. In these reactions, neutrons are produced in pairs,

$$^{18}\mathrm{O} + {}^{4}\alpha \longrightarrow {}^{22}\mathrm{Ne}^{*} \longrightarrow {}^{20}\mathrm{Ne} + 2\mathrm{n}, \tag{3}$$

which together with the high neutron capture efficiency of Gd, helps reduce this source of background for solar neutrinos.

To quantify the production of neutrons from SF and (α, n) reactions, we use the SOURCES-4C code [11]. The neutron production rates for an activity of 1 mBq/kg of each impurity decay chain and 0.2% $Gd_2(SO_4)_3 \cdot 8H_2O$ concentration are shown in Fig. 1 for each decay sub-chain and in Fig. 2 for every relevant reaction. The total expected neutron production rate (events per second) from α decays is then parameterized by:

$$\begin{aligned} R^{\mathrm{rad}}_{\mathrm{neutrons}}(1\mathrm{n}) = \Big(& 2.31 \times 10^{-9} \times \mathcal{C}_{^{238}\mathrm{U}_{\mathrm{early}}} + 0.80 \times 10^{-9} \times \mathcal{C}_{^{238}\mathrm{U}_{\mathrm{late}}} \\ & + 0.02 \times 10^{-9} \times \mathcal{C}_{^{232}\mathrm{Th}_{\mathrm{early}}} + 0.54 \times 10^{-9} \times \mathcal{C}_{^{232}\mathrm{Th}_{\mathrm{late}}} \\ & + 0.20 \times 10^{-9} \times \mathcal{C}_{^{235}\mathrm{U}_{\mathrm{early}}} + 0.78 \times 10^{-9} \times \mathcal{C}_{^{235}\mathrm{U}_{\mathrm{late}}} \Big) \times 0.461 \times m_{\mathrm{FV}}, \end{aligned} \tag{4}$$

where the prefactors on each term (in units of neutrons per second per kg of water per Bq/kg of contamination) represent the total neutron production rate for that sub-chain given the 0.2% $Gd_2(SO_4)_3 \cdot 8H_2O$ concentration and are integrated over the full neutron kinetic energy range. $\mathcal{C}_x$ corresponds to the concentration of radioactive impurities for each part of each decay chain

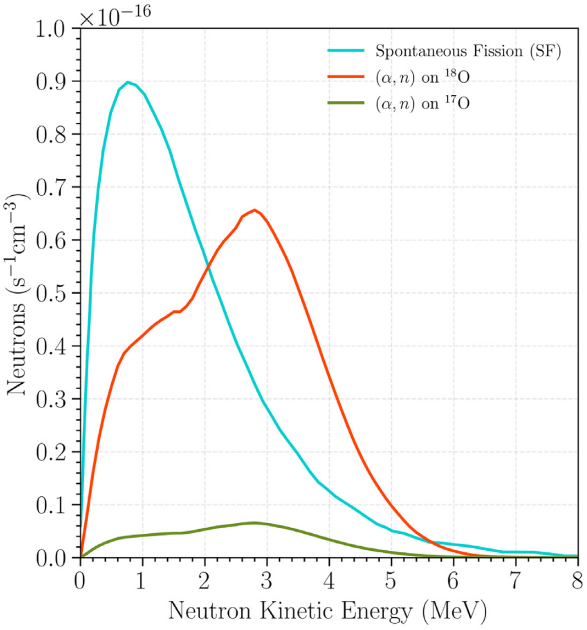

Fig. 2. The neutron production spectrum from each contributing process given 1 mBq/kg of each ^{238}U, ^{232}Th and ^{235}U at a concentration of 0.2% $Gd_2(SO_4)_3 \cdot 8H_2O$.

in units of Bq/kg and the 0.461 factor is the fraction of (α, n) reactions which result in at least one of the two emitted neutrons being captured on gadolinium (90% capture efficiency) but only one reconstructed as a solar neutrino candidate (40% chance to pass SK solar neutrino event cuts).

Background neutrons from (α, n) reactions on ^{18}O impact the solar neutrino analysis at SK. At the impurity concentration imposed on early-chain ^{238}U by the DSNB analysis and on the ^{226}Ra and ^{228}Th chains by β emission as backgrounds to the solar neutrino analysis, the radioactivity-induced neutrons from these chains do not impose any stricter requirements on the impurity concentrations.

For early-chain ^{232}Th, neither SF nor (α, n) reactions on ^{18}O comprise a significant portion of background events on any physics analysis. However, because the half-lives of ^{228}Ra and ^{228}Th are on the same scale as the lifetime of the SK-Gd experiment, we impose the same requirement on the early part of the chain as the one set by β emission on the late part, $<$0.05 mBq/kg.

Similarly, the requirement of ^{235}U is not significantly limited by SF or β emission. To derive a limit on ^{235}U activity we consider that both β emission and radioactivity-induced neutron production contribute to the solar neutrino background. Since the background candidate event rates from β emission of ^{226}Ra and ^{228}Th are together greater than 300 events per day, we limit ^{235}U to as low as reasonably possible. A limit of $<$30 mBq/kg, which is easily achievable through purification, produces around 26 background candidate events per day. We adopt this as the impurity requirement for the entire ^{235}U decay chain.

2.4 *Fluorescence of cerium*

The Cherenkov light wavelength shifting properties of cerium ions have a negative impact on the response of the SK detector. Cerium is typically found in $Gd_2(SO_4)_3 \cdot 8H_2O$ at concentrations at the parts-per-million (ppm) level. The excitation maximum for cerium ions is 255 nm

and the fluorescence emission maximum is around 350 nm with a time constant of around 100 ns [12]. Cherenkov light is emitted in a continuous spectrum that is inversely proportional to the square of the wavelength, and the direction of the photons correlates with the direction of the incoming particles. However, when Cherenkov light near 255 nm, to which the SK photosensors are insensitive, is re-emitted and observed in a random direction with a time constant of 100 ns due to wavelength conversion of cerium, the pattern and time resolution of the longer-wavelength Cherenkov light degrades. Therefore, it is necessary to reduce the cerium concentration in SK-Gd as much as possible.

It was found that the commercially available $Gd_2(SO_4)_3 \cdot 8H_2O$ used in our R&D with the EGADS detector [13] contained about 50 ppm cerium. The observed time distribution of Cherenkov light was distorted significantly by the light emission by cerium. It has been confirmed by EGADS that the hit timing disruption of cerium is not observed when the cerium concentration of $Gd_2(SO_4)_3 \cdot 8H_2O$ is reduced by three orders of magnitude from the nominal value. Therefore, the requirement of cerium content in $Gd_2(SO_4)_3 \cdot 8H_2O$ for SK-Gd was set to 50 parts-per-billion (ppb).

Although gadolinium and cerium are easily separated to the ppm level in the process of refining rare earths, a special treatment is added for a further reduction of cerium to the ppb level or below, which will be explained in Sect. 4.3.

2.5 *Summary of requirements*

SK-Gd aims to measure low-energy neutrinos from the Sun and antineutrinos from the DSNB, nuclear reactors, and the silicon-burning stage prior to a supernova burst. Among them, the solar neutrino and DSNB antineutrino measurements set the strongest requirements on the purity of the $Gd_2(SO_4)_3 \cdot 8H_2O$.

The detection of the DSNB is most strongly limited by ^{238}U SF mimicking an antineutrino IBD signal. Thus, the concentration limit imposed on the early part of the ^{238}U decay chain in $Gd_2(SO_4)_3 \cdot 8H_2O$ is <5 mBq/kg.

Because the ranges of the lowest-energy detectable solar neutrinos and the highest-energy β rays overlap, the detection of solar neutrinos drives the allowable concentration of the ^{232}Th chain, <0.05 mBq/kg, and the late part of the ^{238}U chain, <0.5 mBq/kg. For ^{235}U, the detection of solar neutrinos is most strongly limited by radioactivity-induced neutron production, thereby limiting this nuclide to <30 mBq/kg.

The radioactivity contamination requirements for $Gd_2(SO_4)_3 \cdot 8H_2O$ are summarized in Table 1.

Additionally, once the $Gd_2(SO_4)_3 \cdot 8H_2O$ is dissolved into the water, the uranium concentration is expected to be reduced by approximately two orders of magnitude using the resin-based filtration within the water purification system [13,14]. This has a further positive impact on the measurements affected by uranium contamination.

3. Market production

The world market was searched for suppliers of high-purity $Gd_2(SO_4)_3 \cdot 8H_2O$. Several samples were purchased from different companies to measure and compare their radioactive contaminants. These measurements were performed at Laboratorio Subterráneo de Canfranc (LSC) in Spain (see Sect. 5.1.2), and the results are summarized in Table 2.

Table 1. Summary of contamination requirements of $Gd_2(SO_4)_3 \cdot 8H_2O$ in units of mBq/kg and ppb based on the needs to perform DSNB and solar neutrino analyses. The radioactive decay chains are separated into the early (E) and late (L) sub-chains. The isotopes quoted are the longest lived within each sub-chain, and the values are quoted assuming secular equilibrium (eq.) within that sub-chain.

Chain	Part of chain	Requirement (mBq/kg)	Requirement (ppb)[1]
^{238}U	E, ^{238}U eq.	<5	<0.4
	L, ^{226}Ra eq.	<0.5	
^{232}Th	E, ^{232}Th eq.	<0.05	<0.013
	L, ^{228}Th eq.	<0.05	
^{235}U	E, ^{235}U eq.	<30	<50
	L, ^{227}Ac eq,	<30	
	Ce	–	<50

[1]ppb values are in units of kg/kg and corrected assuming each isotope's natural abundance.

Table 2. Radioactivity in samples of $Gd_2(SO_4)_3 \cdot 8H_2O$ obtained from different suppliers at different times, as measured at the LSC. Activities presented are in units of mBq/kg and limits are at 95% confidence limit. The measurements of the radioactive chains are separated into those for the early part of the chain (E) and the late part of the chain (L). The isotopes quoted are the longest lived within the sub-chain, and the activities are estimated assuming equilibrium (eq.)

		^{238}U chain		^{232}Th chain		^{235}U chain		Others		
Company	Date	E, ^{238}U eq.	L, ^{226}Ra eq.	E, ^{228}Ra eq.	L, ^{228}Th eq.	E, ^{235}U eq.	L, ^{227}Ac eq.	^{40}K	^{138}La	^{176}Lu
A (USA)	2009/04	51 ± 21	8 ± 1	11 ± 2	28 ± 3	<32	214 ± 10	29 ± 5	8 ± 1	80 ± 8
A (USA)	2010/08	<33	2.8 ± 0.6	270 ± 16	86 ± 5	<32	1700 ± 20	12 ± 3	–	21 ± 2
B (China)	2012/08	292 ± 6	74 ± 2	1099 ± 12	504 ± 6	<112	2956 ± 30	101 ± 10	683 ± 15	566 ± 6
C (China)	2013/02	74 ± 28	13 ± 1	205 ± 6	127 ± 3	<25	1423 ± 21	60 ± 7	3 ± 1	12 ± 1
B (China)	2013/03	242 ± 6	13 ± 2	21 ± 3	374 ± 6	<25	175 ± 42	18 ± 8	42 ± 3	8 ± 2
A (USA)	2013/08	71 ± 20	8 ± 1	6 ± 1	159 ± 3	<32	295 ± 10	3 ± 2	5 ± 1	30 ± 1
D (China)	2013/07	47 ± 26	5 ± 1	14 ± 2	13 ± 1	<12	<6	3 ± 2	<1	1.6 ± 0.3
D (China)	2013/07	73 ± 27	6 ± 1	3 ± 1	411 ± 5	<30	<18	8 ± 4	<1	<2
A (USA)	2014/02	<76	<1.4	2 ± 1	29 ± 2	<1.8	190 ± 6	<5	23 ± 1	2.5 ± 0.6

These measurements indicate the presence of nonnegligible naturally occurring radioactive contamination in the material, much higher than the requirements discussed in the previous section. It is worth noting that, as expected, the early and late parts of the radioactive decay chains do not appear to be in secular equilibrium. Also, as already mentioned in Sect. 2.4, some of the $Gd_2(SO_4)_3 \cdot 8H_2O$ samples used in our R&D contained unacceptable amounts of cerium, near the natural abundance of cerium in the Earth's crust.

All the above clearly shows that a dedicated R&D program must be carried out to purify the available $Gd_2(SO_4)_3 \cdot 8H_2O$ powder to levels which satisfy the requirements in Table 1.

4. Purification method

4.1 *Gadolinium oxide and its solution by acid*

Gadolinium oxide, Gd_2O_3, is used as a raw material for $Gd_2(SO_4)_3 \cdot 8H_2O$ production. The purity of Gd_2O_3 is better than 99.99% by mass as Gd_2O_3/TREO (gadolinium oxide amount in total rare earth oxide amount). The concentration of trace uranium and thorium contained in Gd_2O_3 with this purity is typically about 500–1000 ppb, but we carefully selected raw material with a low thorium concentration (150−200 ppb) for this development.

To dissolve Gd_2O_3, hydrochloric acid is used. This is because gadolinium chloride, $GdCl_3$, has a high solubility, and wastewater treatment is relatively easy since it does not contain nitrogen. This gadolinium acidic aqueous solution becomes a raw material for the subsequent production process after the insoluble matter is filtered off. The acid concentration is set to 30–40% by weight, resulting in high reactivity and low volatility. From the viewpoint of the removal efficiency of radioactive impurities and the yield in the subsequent processes, the target gadolinium concentration in this solution is then ∼305 g/L (Gd_2O_3: 350 g/L).

4.2 *Solvent extraction*

The solution obtained above is then processed by solvent extraction to increase the purity. While maintaining gadolinium in the aqueous phase, radioactive impurities such as thorium and uranium can be extracted into the organic solvent phase using extractant 2-ethylhexyl 2-ethylhexylphosphonate (PC-88A manufactured by Daihachi Chemical Industry Co., Ltd.). Rare earth elements can be extracted and separated in an organic solvent containing 2-ethylhexylphosphonate [15]. The extraction solvent is diluted with an isoparaffin (IP3835 manufactured by Idemitsu Kosan Co., Ltd.) which reduces the viscosity and specific gravity of the organic solvent phase. Reducing the viscosity improves contact between the aqueous phase and the organic solvent phase to improve the efficiency of solvent extraction. Reducing the specific gravity accelerates the separation between the organic solvent phase and the aqueous phase after mixing. The extraction solvent and the isoparaffin solvent are mixed at a volume ratio of 20:80.

Between a pH of 1.0 and 1.3, gadolinium is not extracted into the organic solvent phase, but thorium and uranium are. During this process, the pH is controlled at 1.0 by using an ammonia solution to prevent metal contamination and enhance separation efficiency. After mixing the isoparaffin with the aqueous solution, the aqueous phase is separated as a purified gadolinium solution by allowing the mixed solution to separate. This solvent extraction step is performed twice for this production.

4.3 *Neutralization and sulfation*

After solvent extractions, two neutralization processes are performed to reduce the thorium and cerium levels. Because the precipitation pH of thorium hydroxide is lower than the precipitation pH of gadolinium hydroxide, thorium hydroxide can be removed by coprecipitating with a small amount of gadolinium hydroxide by adjusting pH. The pH is adjusted to 4.8 by adding ammonia water to the gadolinium solution after the solvent extraction. In an acidic solution, cerium is trivalent and stable but it was precipitated as cerium oxide by adding hydrogen peroxide solution and raising the electric potential in the solution to oxidize it. By performing this treatment together with the precipitation of thorium hydroxide described above, cerium oxide is coprecipitated together with thorium hydroxide. Hydrogen peroxide is added so that it is 0.3% in the aqueous solution.

Finally, 98% purity sulfuric acid is added to the obtained gadolinium solution to precipitate gadoliniumsulfate. Gadolinium sulfate is filtered to remove the filtrate, and washed with pure water until the pH reaches 4. The produced gadolinium sulfate is octahydrate. This can be confirmed by X-ray diffraction (Appendix A) or thermogravimetric analysis (Appendix B).

Each batch of the $Gd_2(SO_4)_3 \cdot 8H_2O$ production is about 500 kg. The $Gd_2(SO_4)_3 \cdot 8H_2O$ is in a powder form but contains an average of 2.5% additional water left over from process-

(a) (b)

Fig. 3. (a) The BUGS Facility at Boulby Underground Laboratory and (b) a 5-kg $Gd_2(SO_4)_3 \cdot 8H_2O$ sample on the Merrybent detector.

ing. So the 13.2 metric tons of powder dissolved into SK corresponds to 12.9 metric tons of $Gd_2(SO_4)_3 \cdot 8H_2O$.

5. Material assay

Samples from each 500-kg batch of $Gd_2(SO_4)_3 \cdot 8H_2O$ are assayed to evaluate whether the requirements set out in Sect. 2 for radioactive and fluorescent impurities are met. Since the nuclides which contaminate $Gd_2(SO_4)_3 \cdot 8H_2O$ are not necessarily in secular equilibrium with their long-lived parents and daughters, high-purity germanium (HPGe) γ spectrometry is used to investigate the activity of the early and late parts of all decay chains which could affect SK-Gd physics sensitivities. Also, inductively coupled plasma mass spectrometry (ICP-MS) is used to measure the concentrations of uranium, thorium, and cerium to very low levels.

ICP-MS is sensitive to the most abundant, long-lived members of the early parts of the uranium and thorium decay chains to the level required by SK-Gd: ^{238}U to <5 mBq/kg and ^{232}Th to <0.05 mBq/kg. HPGe γ spectrometry infers the activity of long-lived parent nuclides based on the γ emission of the parent or its daughters. For late-chain ^{238}U (^{226}Ra equilibrium) and all parts of the ^{235}U chain, only HPGe γ spectrometry is sensitive to the level specified by the SK-Gd requirements: <0.5 mBq/kg and <30 mBq/kg, respectively. Neither method of assay used here is sensitive to late-chain ^{232}Th (^{228}Th equilibrium) concentrations of <0.05 mBq/kg.

5.1 *HPGe laboratories*

5.1.1 *Boulby.* The Boulby UnderGround Screening (BUGS) Facility [16] (Fig. 3a) is located 1.1 km underground (2840 m water equivalent) at the Boulby Underground Laboratory in the north of England. γ spectrometry of 13 samples of $Gd_2(SO_4)_3 \cdot 8H_2O$ was performed using two HPGe detectors at BUGS. Produced by Mirion, the two p-type detectors, called Belmont and Merrybent, have relative efficiencies of 160% and 100%, respectively. The "specialty ultra-low background" detectors are housed in similar low-background lead and inner copper-lined shields and are purged with generated nitrogen gas. Additional details of these detectors and their general performance around the same time as this assay program are reported in Ref. [17].

Samples of 5 kg of $Gd_2(SO_4)_3 \cdot 8H_2O$ were packed in Marinelli beakers of type 448G-E from Ga-Ma and Associates, Inc. in a clean environment, then transported into the BUGS class 1000

(a) (b) (c)

Fig. 4. (a) ULBS laboratory in Hall C of LSC, (b) a $Gd_2(SO_4)_3$ sample inside the GeOroel shield, and (c) a $Gd_2(SO_4)_3 \cdot 8H_2O$ sample inside the Asterix shield.

clean room using standard triple-bagged procedures. Figure 3(b) shows a $Gd_2(SO_4)_3 \cdot 8H_2O$ sample placed on the Merrybent detector. Samples are measured for several weeks to reach a minimum detectable activity (MDA) of $<$0.5 mBq/kg of ^{226}Ra-equivalent activity at the 95% confidence level.

To achieve the best possible results, several known systematic errors are accounted for in the spectrum analysis using a Geant4-based [18] detector simulation developed in-house. Apart from estimating the γ detection efficiency for an arbitrary sample geometry, corrections for true coincidence summing [16] and background shielding by the sample material [19] are implemented to improve the accuracy of results.

Since this assay program has been completed, several improvements have been made at BUGS to reduce the radon concentration of the nitrogen purge line, greatly improving the sensitivity of Merrybent and Belmont to ^{226}Ra and its daughters.

5.1.2 *LSC.* The LSC is located on the Spanish side of the Pyrenees Mountains, under the Tobazo peak. The laboratory has a rock shielding of 800 water equivalent), which suppresses the cosmic muon flux by almost 5 orders of magnitude.

The Ultra-Low Background Service (ULBS), working since 2010 in Hall C of LSC (Figure 4a), offers a high-quality material assay facility to experiments. At present, it is equipped with six 2-kg p-type coaxial HPGe detectors with $\sim$ 100% relative efficiency and two SAGe-Well High-Purity detectors, shielded with 20 cm of lead with a low contamination in ^{210}Pb. An internal 10-cm layer of oxygen-free high thermal conductivity copper completes the shielding. For SK-Gd, two p-type detectors were mainly used: GeOroel and Asterix (see Table 3).

Samples of $\sim$4 kg $Gd_2(SO_4)_3 \cdot 8H_2O$ were packed in Marinelli beakers (Ga-Ma and Associates, Inc., model 445N-E). Measurements of around 30 days are necessary to reach mBq/kg sensitivity, with the condition that the radon contained in the air inside the HPGe detector shielding has decayed. To achieve this, each detector has an extra layer of shielding made of methacrylate which surrounds the lead shielding. To impede the exterior air (and the radon) from entering inside the shielding, a slight overpressure is created inside the copper shielding. The copper shield inner volume available for sample measurement is $\sim$43 l (see Fig. 4(b) and 4(c)). This volume is flushed with $\sim$274 l/h of a mixture of nitrogen and radon-free air, which corresponds to about six full volume changes per hour.

Table 3. HPGe detectors used and their main properties and background characteristics. The number of samples assayed by each detector is also shown, including batches measured but not selected for use in SK-Gd.

				Counts (/kg/day)					
Lab	Detector	Mass (kg)	FWHM@ 1332 keV (keV)	Integral 60–2700 keV	^{208}Tl, 2614 keV	^{214}Bi, 609 keV	^{60}Co, 1332 keV	^{40}K, 1461 keV	SK-Gd total samples
BUGS	Belmont	3.2	1.92	90.0	0.12	0.67	0.47	0.58	8
BUGS	Merrybent	2.0	1.87	145.0	0.23	2.15	0.47	1.16	5
LSC	GeOroel	2.31	2.22	128.7	0.53	0.89	0.06	0.46	3
LSC	Asterix	2.13	1.92	171.3	0.11	1.10	0.28	0.61	13
LSC	GeAnayet	2.26	1.99	461.2	3.68	0.71	0.16	0.74	2
Kamioka	Lab-C Ge	1.68	2.39	104.5	0.08	0.39	0.41	0.44	23

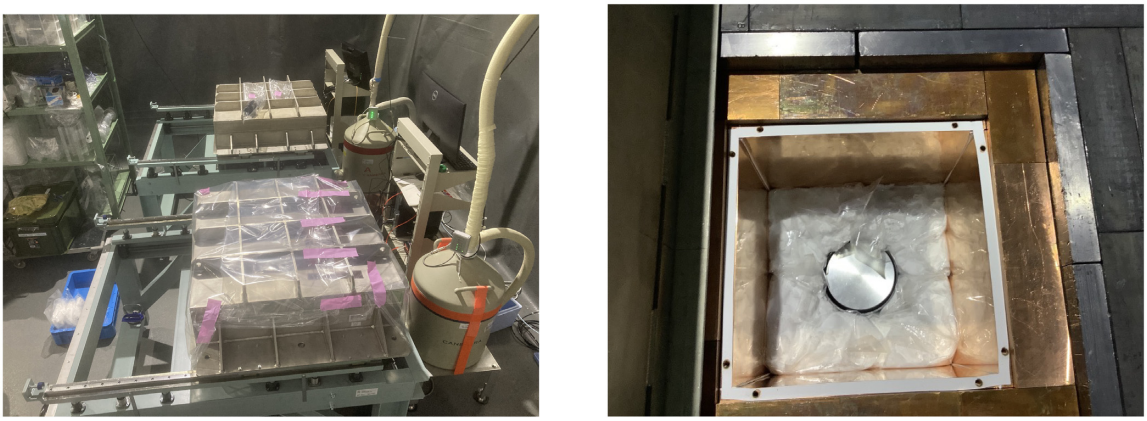

(a) (b)

Fig. 5. (a) Germanium detectors in Lab-C at Kamioka Observatory, (b) Kamioka Lab-C germanium detector with 10 kg of $Gd_2(SO_4)_3 \cdot 8H_2O$ in EVOH bags loaded for measurement.

5.1.3 *Kamioka.* Kamioka Observatory is located 2700 m water equivalent underground. In addition to housing the SK-Gd detector, several HPGe detectors are operated to support the many scientific goals of the laboratory. For the current $Gd_2(SO_4)_3 \cdot 8H_2O$ assay program, the ultra-low background HPGe detector located in Lab-C, manufactured by Mirion Technologies France [20], was used. Details of the shield geometry and detector performance can be found in Ref. [21].

Samples of $Gd_2(SO_4)_3 \cdot 8H_2O$ are prepared in two ways. First, a molecular recognition resin embedded in the "Empore Radium Rad Disk" [22,23] was used to adsorb radium from the $Gd_2(SO_4)_3 \cdot 8H_2O$ and increase its concentration. Since the size of the disk is small (47 mm diameter, 0.5 μm thickness), it could be laid directly onto the end cap of the HPGe detector to measure the concentrated radium activity in $Gd_2(SO_4)_3 \cdot 8H_2O$ with high detection efficiency. A ^{226}Ra activity of 0.5 mBq/kg is measurable with ten days of measurement using this method.

Second, 2.5 kg of $Gd_2(SO_4)_3 \cdot 8H_2O$ was packed into ethylene-vinyl alcohol (EVOH) bags. Any radon present was purged from the bags with radon-free air, the bags evacuated and then closed. Four such bags are loaded directly into the HPGe shield, surrounding the detector head and filling the space within the shield. Figure 5(b) shows the detector with four EVOH bags of

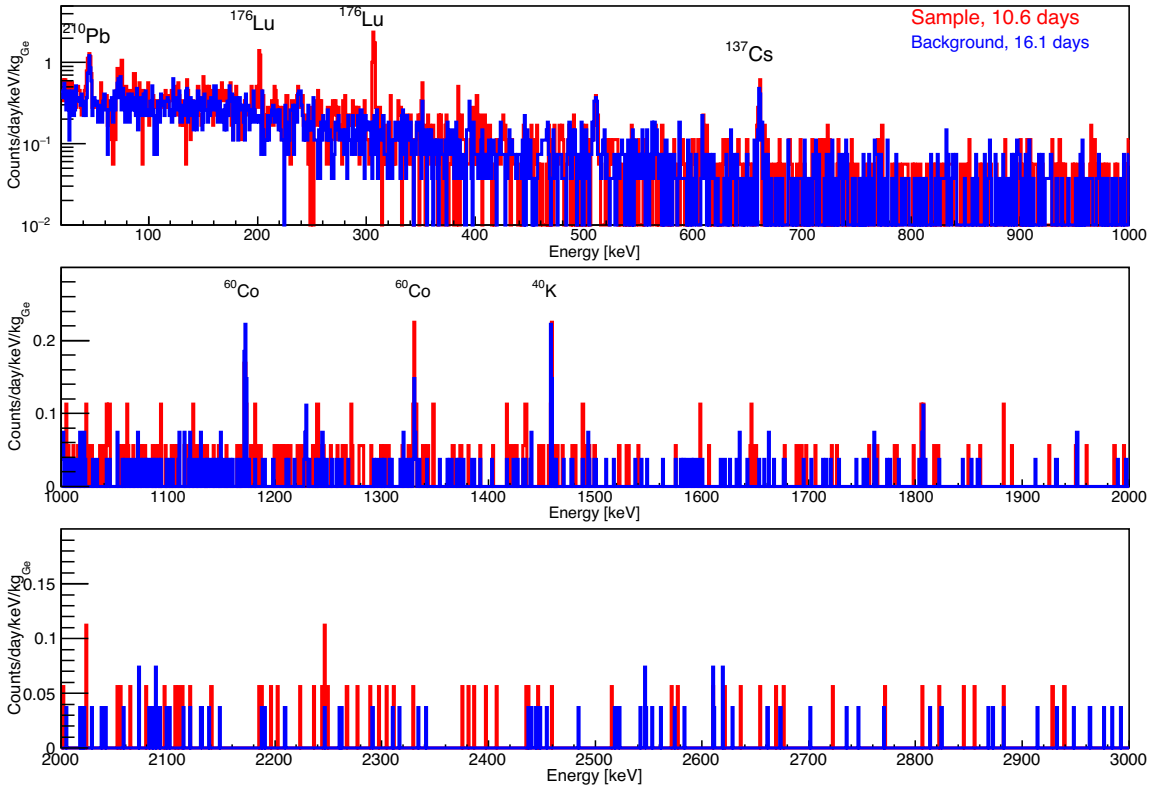

Fig. 6. A typical γ spectrum (red) corresponding to 10 kg of $Gd_2(SO_4)_3 \cdot 8H_2O$ measured by Kamioka's Lab-C germanium detector, and the detector background (blue). The 662 keV peak related to ^{137}Cs arises from contamination in the shield materials. The ^{60}Co peaks originate from cosmogenic neutron activation of the copper shield material.

$Gd_2(SO_4)_3 \cdot 8H_2O$ loaded for measurement. About two weeks of sample measurement time is required to achieve a MDA of $<$0.5 mBq/kg of ^{226}Ra at 95% confidence level.

A Monte Carlo simulation based on Geant4 was used to evaluate the detection efficiency for the sample geometries.

5.2 *HPGe performance*

Table 3 shows relevant characteristics and some background count rates at relevant γ energies of all the HPGe detectors used, as well as the number of SK-Gd samples assayed on each.

Figure 6 shows a typical measurement spectrum (red) compared with the detector background (blue). The measurement corresponds to 10 kg of $Gd_2(SO_4)_3 \cdot 8H_2O$ measured by Kamioka's Lab-C Ge detector. No peaks from daughters of ^{226}Ra (for example, ^{214}Pb: 295 keV, 352 keV, and ^{214}Bi: 609 keV, 1120 keV, 1764 keV) are observed either in the sample or background data. The two peaks observed at 202 keV and 307 keV in the sample spectrum come from the decay of ^{176}Lu, which is observed in most $Gd_2(SO_4)_3 \cdot 8H_2O$ samples.

A true comparison of the sensitivities of the HPGe detectors accounts for the detector backgrounds as well as the γ detection efficiency for the particular sample. For $Gd_2(SO_4)_3 \cdot 8H_2O$ samples prepared according to the particular procedures used in each laboratory, all of the detectors used in this study are sensitive to $<$30 mBq/kg of ^{235}U and its daughters within just a few days of measurement. In contrast, none of the HPGe detectors are sensitive to $<$0.05 mBq/kg of ^{232}Th daughters in any realistic measurement timescale (see Fig. 7(b)). Since ^{238}U is measur-

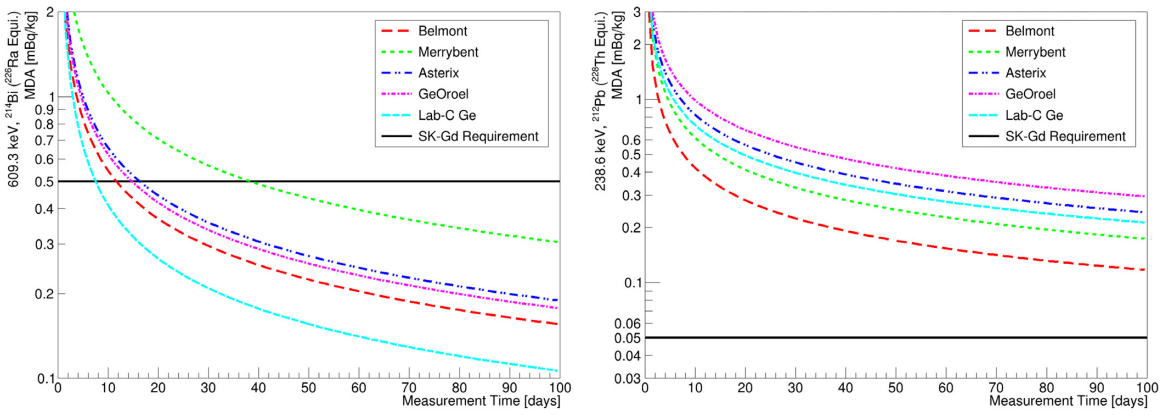

(a) (b)

Fig. 7. The minimum detectable activity (MDA) for (a) the 609.3 keV γs from ^{214}Bi and (b) the 238.6 keV γs from ^{212}Pb for five HPGe detectors in this study. The solid black lines represent the SK-Gd requirement for the respective mean impurity activity.

able using ICP-MS, achieving a sensitivity of $<$5 mBq/kg using HPGe methods is not critical. For ^{226}Ra daughters, all HPGe detectors are sensitive to $<$0.5 mBq/kg within a few weeks of measurement (see Fig. 7(a)). It is this requirement which primarily motivates the measurement time of $Gd_2(SO_4)_3 \cdot 8H_2O$ samples on the HPGe detectors.

5.3 *ICP-MS*

In addition to HPGe gamma spectrometry at Kamioka Laboratory, specialty ICP-MS is used to assay uranium, thorium, and cerium impurities.

To measure uranium and thorium at the parts-per-trillion (ppt) level, a solid-phase extraction technique has been developed [22]. First, a nitric acid aqueous solution in which a sample of $Gd_2(SO_4)_3 \cdot 8H_2O$ is dissolved is passed through a well-washed chromatographic extraction resin, so that about 90% or more uranium and thorium are adsorbed on the resin but gadolinium is not. Uranium and thorium can then be eluted from the resin when a dilute nitric acid solution is passed through. Finally, by analyzing the elute with ICP-MS it is possible to measure trace amounts of uranium and thorium without interference from gadolinium, which is reduced by a factor of about 10^4.

To assay cerium impurities, $Gd_2(SO_4)_3 \cdot 8H_2O$ is diluted 10,000-fold by mass ratio with 2% HNO_3. Then the concentration of cerium in the aqueous solution is directly measured using ICP-MS. At this concentration, the matrix effect due to the existence of gadolinium is negligible because the gadolinium concentration is 0.01%.

6. Results

Table 4 shows the results from the ICP-MS assays of all batch samples of $Gd_2(SO_4)_3 \cdot 8H_2O$. All samples meet the criteria for uranium, thorium and cerium contamination except for one which slightly exceeds the criteria value for thorium. This will be discussed later in more detail. The mean cerium concentration in all approved samples of $Gd_2(SO_4)_3 \cdot 8H_2O$, weighted by the dissolved batch mass, is measured to be 11.1 ± 3.8 ppb, well below the 50 ppb requirement.

γ spectrometric assay results for all SK-Gd batch samples are shown in Table 5. For the late-chain ^{238}U (^{226}Ra equilibrium) and entire ^{235}U series, most of the limits set on the activity

Table 4. Results from ICP-MS assays of all samples taken from batches which have been approved for use in SK-Gd. The SK requirement on the concentration of each element is indicated at the top of each column.

Sample	Ce (ppb) <50	U (ppt) <400	Th (ppt) <13
17090X	35 ± 1.6	<2.7	4.9 ± 1.8
180702	<10	<3.0	4.8 ± 0.4
180703	<10	<1.4	9.1 ± 2.9
190302	23.5 ± 1.0	<6.4	<9.8
190303	10.4 ± 1.2	<7.3	<19
190304	10.8 ± 0.7	<13	<19
190502	10.0 ± 0.6	<4.9	<7.4
190604	32.5 ± 0.7	4.8 ± 0.5	7.7 ± 0.7
190606	29.0 ± 0.8	<8.9	<17
190607	10.1 ± 0.1	<9.7	11.6 ± 2.3
190608	13.8 ± 1.0	<5.6	<7.7
190702	12.1 ± 0.7	3.9 ± 0.3	<12
190703	9.7 ± 0.6	3.4 ± 0.6	2.1 ± 0.4
190704	13.9 ± 0.5	5.9 ± 0.4	6.3 ± 0.8
190706	5.3 ± 0.6	4.7 ± 0.4	1.2 ± 0.1
190801	4.5 ± 0.5	3.7 ± 0.4	2.1 ± 0.8
190803	6.3 ± 0.6	3.4 ± 0.6	1.9 ± 0.6
190804	6.0 ± 0.3	2.5 ± 0.7	15.5 ± 1.0
190805	6.5 ± 0.6	2.2 ± 0.8	0.2 ± 0.3
190806	5.9 ± 0.4	8.5 ± 1.0	7.8 ± 0.5
190901	8.0 ± 0.9	4.0 ± 0.3	7.2 ± 1.0
190902	5.7 ± 0.4	2.4 ± 0.5	5.0 ± 1.1
190903	5.5 ± 0.4	4.0 ± 1.0	3.8 ± 0.5
190905	6.5 ± 0.4	2.7 ± 0.5	4.4 ± 0.7
200101	6.7 ± 0.8	<4.2	<6.5
200103	4.5 ± 0.2	1.4 ± 0.3	2.1 ± 0.5
200104	4.0 ± 0.4	1.4 ± 0.5	2.5 ± 0.9

are below the detection limit for the given detector. Some activities in these sub-chains are reported with finite, nonzero values at the 95% confidence level. The decision criteria for reporting one-sided or two-sided confidence intervals for low numbers of counts follows the procedure recommended in Ref. [24].

For ^{228}Ra and ^{228}Th, many of the later batches (after 190706) are observed to contain more than the criterion value of γ activity. Because the measurements of ^{232}Th indicate an activity which satisfies the SK-Gd requirements, it is inferred that the production and processing of the $Gd_2(SO_4)_3 \cdot 8H_2O$ powder disrupts the secular equilibrium in the decay chain, removing ^{232}Th more efficiently than ^{228}Ra. The significant excess of ^{228}Ra daughters in these later batches is associated with a known excess of impurities in the raw material Gd_2O_3 which was used to produce these batches. As described in Sect. 4, most lots of Gd_2O_3 were selected to contain 150–200 ppb of Th. The later lots contained more thorium but could not be affordably replaced with a cleaner raw material. We justify the use of this material, despite the impurities, knowing that radium is adsorbed by cation exchange resins in the SK-Gd water system [14], and that the mean lifetime of ^{228}Th is 2.7 years, well within the expected lifetime of the SK-Gd project.

Table 5. Summary of $Gd_2(SO_4)_3 \cdot 8H_2O$ assay results by HPGe detectors. The sample identifier is coded as follows: YYMM##, where YYMM is the year and month of production and ## refers to the batch number produced within that month. The measurements of each radioactive chain are separated into the early part of the chain (E) and the late part of the chain (L). The isotopes identified are the longest lived within each sub-chain, and the activities are estimated assuming secular equilibrium (eq.) within each sub-chain.

Sample	Laboratory	Detector/method	Activity (mBq/kg, 95% CL)										
			^{238}U chain		^{232}Th chain		^{235}U chain		^{40}K	^{138}La	^{176}Lu	^{134}Cs	^{137}Cs
			E,^{238}U eq.	L,^{226}Ra eq.	E,^{228}Ra eq.	L,^{228}Th eq.	E,^{235}U eq.	L,^{227}Ac eq.					
		SK-Gd Req. →	<5	<0.5	<0.05	<0.05	<30	<30	–	–	–	–	–
17090X	LSC	Asterix	<8.4	<0.21	<0.30	<0.30	<0.42	<1.6	<1.0	<0.14	0.13±0.03	<0.07	<0.13
180702	LSC	Asterix	<4.3	<0.12	<0.22	<0.21	<0.3	<1.1	<0.5	0.13±0.04	0.24±0.03	<0.07	<0.08
180703	LSC	Asterix	<6.3	<0.24	<0.44	<0.38	<0.3	<1.1	<0.5	<0.14	0.22±0.03	<0.07	<0.07
190302	LSC	Asterix	<6.7	<0.32	<0.35	<0.29	<0.42	<0.92	<1.6	0.26±0.1	<0.21	<0.09	<0.09
190303	LSC	Asterix	<5.9	<0.3	<0.44	<0.29	<0.39	<0.81	<1.5	0.45±0.09	0.16±0.12	<0.08	<0.09
190304	LSC	Asterix	<7.7	<0.42	<0.55	<0.36	<0.52	<1.22	<2.1	0.40±0.11	<0.21	<0.13	<0.14
190502	Boulby	Belmont	<5.4	<0.49	<0.95	<0.48	<0.36	<1.7	<2.8	<0.28	0.49±0.08	–	<0.10
190502	Kamioka	Lab-C Ge	<25.0	<0.75	<0.52	<0.36	<9	7.9±0.8	<1.63	<0.37	0.68±0.18	<0.16	<0.22
190604	Boulby	Belmont	<9.80	<0.47	<0.61	<0.50	<0.45	<2.33	<2.45	<0.21	0.97±0.11	–	<0.08
190604	Kamioka	Lab-C Ge	<26.9	<0.68	<0.55	<0.33	<4.6	<1.2	<2.02	<0.36	1.43±0.19	<0.19	<0.34
190606	Boulby	Merrybent	<13.1	<0.84	<0.79	<0.63	<0.37	2.6±0.6	<3.27	<0.29	1.23±0.16	–	<0.13
190606	Kamioka	Lab-C Ge	<17.3	<1.36	<0.91	<0.94	<8.3	2.6±1.3	<3.20	<0.26	0.74±0.29	<0.39	<0.50
190606	Kamioka	Lab-C Ge, Ra Disk	–	<0.31	<0.82	<0.48	–	–	–	–	–	–	–
190607	LSC	GeOroel	<5.0	<0.30	<0.79	<0.42	<0.30	<0.96	<1.59	<0.18	<0.13	<0.12	<0.09
190608	LSC	Asterix	<6.2	<0.53	<0.43	<0.35	<0.40	<0.88	<1.50	<0.14	<0.25	<0.08	<0.09
190608	Kamioka	Lab-C Ge	<23.2	<1.06	<1.38	<0.80	<4.3	<1.8	<2.15	<0.49	<0.51	<0.21	<0.30
190608	Kamioka	Lab-C Ge, Ra Disk	–	<0.63	<0.52	<0.61	–	–	–	–	–	–	–
190702	LSC	GeOroel	<7.7	<0.45	<1.11	<0.50	<0.37	2.4±0.9	<1.5	<0.20	0.23±0.13	<0.12	<0.11
190702	Kamioka	Lab-C Ge	<12.0	<0.63	<1.08	<0.33	<3.4	<1.6	<1.99	<0.28	0.28±0.12	<0.17	<0.28
190703	LSC	Asterix	<5.9	<0.35	<0.51	<0.50	<0.45	1.8±1.0	<1.7	<0.20	0.51±0.13	<0.10	<0.10
190704	Boulby	Belmont	<9.8	<0.44	<0.66	<0.75	<0.29	<1.39	<2.01	<0.25	<0.18	–	<0.10
190706	Boulby	Belmont	<9.5	<0.45	<0.66	0.53±0.12	<0.28	<1.32	<2.09	<0.25	<0.25	–	<0.13
190706	Kamioka	Lab-C Ge	<9.4	<0.69	<0.50	<0.86	<2.26	<1.10	<1.9	<0.29	<0.19	<0.19	<0.26
190801	LSC	GeAnayet	<20	<0.92	<1.5	<0.77	<0.80	<1.17	<1.44	<0.18	2.7±0.2	<0.23	<0.18
190803	LSC	Asterix	<4.9	<0.31	0.39±0.21	0.55±0.22	<0.36	<0.74	<1.4	<0.09	3.5±0.1	<0.08	<0.07
190804	Boulby	Belmont	<11	<0.46	0.67±0.21	<0.67	<0.38	<1.98	<2.57	<0.20	4.60±0.24	–	<0.10
190805	LSC	GeOroel	<6.5	<0.52	0.53±0.44	0.57±0.40	<0.44	<0.98	<1.18	<0.10	9.44±0.10	<0.10	<0.09
190806	Boulby	Merrybent	<8.09	<0.43	0.49±0.11	1.27±0.13	<0.26	<1.23	<1.78	<0.14	9.35±0.22	–	<0.07
190901	LSC	Asterix	<6	<0.30	0.42±0.27	0.37±0.27	<0.46	<1.20	<1.47	<0.15	4.85±0.12	<0.10	<0.13
190902	Boulby	Belmont	<5.52	<0.26	0.53±0.10	0.63±0.09	<0.33	<1.22	<1.32	<0.10	8.78±0.18	–	<0.05
190903	LSC	Asterix	<6.2	<0.37	0.59±0.28	0.35±0.28	<0.54	<1.7	<1.5	<0.14	4.9±0.1	<0.10	<0.09
190905	Kamioka	Lab-C Ge	<8.6	<0.21	0.72±0.20	0.70±0.16	<5.2	<1.1	<1.57	<0.09	6.6±0.2	<0.09	<0.13
190905	Kamioka	Lab-C Ge, Ra Disk	–	<0.29	0.58±0.25	<0.39	–	–	–	–	–	–	–
200101	Kamioka	Lab-C Ge	<6.80	<0.35	0.98±0.18	1.00±0.15	8.24±1.68	<0.54	<0.95	<0.08	6.25±0.17	<0.18	<0.13
200103	Kamioka	Lab-C Ge	<8.46	0.51±0.12	1.42±0.25	0.84±0.17	<2.11	<0.88	<1.43	<0.12	0.18±0.07	<0.13	<0.16
200104	Kamioka	Lab-C Ge	<8.39	<0.36	1.48±0.24	0.84±0.18	<3.45	<0.95	<1.02	<0.08	<0.28	<0.23	<0.11

Table 6. Summary of HPGe and ICP-MS measurement results for all samples of $Gd_2(SO_4)_3 \cdot 8H_2O$ assayed and approved for dissolving into SK, compared with the total SK-Gd radioactivity budget assuming 0.2% loading of 130 metric tons of $Gd_2(SO_4)_3 \cdot 8H_2O$. The measurements of each radioactive chain are separated into those for the parent radioactive isotopes (RIs), the early part of the chain (E) and the late part of the chain (L). The HPGe assay results are combined in two ways to give an estimate of the minimum and maximum total added radioactivity to SK.

Chain	Part of Chain	$t_{1/2}$	SK-Gd requirement		HPGe		ICP-MS
			Specific activity (mBq/kg)	Total budget (Bq)	FM (Bq)	UL (Bq)	Total (Bq)
^{238}U	RI ^{238}U	4.5 Gy	<5	650	–	–	0.34 ± 0.15
	E, ^{238}U eq.	4.5 Gy	<5	650	0	<89	–
	L, ^{226}Ra eq.	1602 y	<0.5	65	0.25 ± 0.06	<5.2	–
^{232}Th	RI ^{232}Th	14 Gy	<0.05	6.5	–	–	0.25 ± 0.07
	E, ^{228}Ra eq.	5.7 y	<0.05	6.5	4.1 ± 0.4	<11	–
	L, ^{228}Th eq.	1.9 y	<0.05	6.5	3.8 ± 0.3	<8.9	–
^{235}U	E, ^{235}U eq.	0.7 Gy	<30	3900	4.1 ± 0.8	<15	–
	L, ^{227}Ac eq.	21.7 y	<30	3900	3.3 ± 0.7	<19	–

We also note that many samples contained ^{176}Lu and ^{138}La. Since these nuclides have Q-values below 2 MeV, they are below the detection threshold in SK-Gd so do not meaningfully affect any physics analyses.

The total impurity activity budget for SK-Gd (Sect. 2) is generally based on the requirement that backgrounds will not increase by more than 100% of the pre-gadolinium backgrounds. For all of the limited decay chain activities, the radioactivity budget is shown in Table 6 along with a summary of the estimated total impurities dissolved into SK-Gd via the $Gd_2(SO_4)_3 \cdot 8H_2O$.

To estimate the total impurities in all batches, we first assume that each small (4–10 kg for HPGe measurements, several grams for ICP-MS measurements) assayed sample exactly represents the radioactivity of the full 500-kg batch from which it came, then combine the finite activities and upper limits in two ways. First, a lower bound on the total activity is the sum of all finite measured (FM) activities, with the errors combined in quadrature. Second, a conservative upper bound on the total activity is the sum of all 95% confidence level upper limits (UL), which includes the reported one-sided confidence intervals as well as the finite measurements plus 1.645 times the measurement standard deviation.

For ^{238}U and ^{232}Th, the ICP-MS measurements show that the total added radioactivity is well below the SK-Gd budget. The HPGe results for all parts of the ^{238}U and ^{235}U decay chains show that, even in the worst-case scenario, the SK-Gd requirements are met even though some samples of $Gd_2(SO_4)_3 \cdot 8H_2O$ contain activities which exceed the required specific activity for these nuclides.

For ^{228}Ra and ^{228}Th, the sum of FM activities in all batch samples is more than half of the total SK-Gd budget, even though these dissolved batches only consist of about 10% of the design gadolinium concentration. The conservative UL activities for these decay chains are 30% to 60% greater than the total SK-Gd budget. Without better measurements of the ^{228}Ra and ^{228}Th activities, it is not known whether the SK-Gd total budget is met or exceeded.

Table 7. Relevant chemical properties during gadolinium processing with and without the new purification procedures.

	Only solvent extraction	With hydroxide precipitation
pH during precipitation	–	8.0
pH during solvent extraction	1.1	1.1
Gadolinium recovery rate (%)	91	90
^{238}U by ICP-MS (ppb)	16	<0.8
^{232}Th by ICP-MS (ppb)	1.2	<0.02
^{228}Ra by HPGe (mBq/kg)	162	<0.4

Since the ^{232}Th activity is shown to be well within the total SK-Gd budget, and since it is known that radium is adsorbed by the resin in the SK-Gd water system, only the observed activity of ^{228}Th is expected to be problematic for SK-Gd. The HPGe result for ^{228}Th represents the true activity of ^{208}Tl at the time of measurement, which will decay with a 1.9-yr half-life assuming all ^{228}Ra is removed during the SK-Gd water filtration. By one half-life, the worst-case estimate of total ^{208}Tl activity is within the SK-Gd requirement.

7. New purification process to reduce radium

To reduce the radium concentration in future batches of $Gd_2(SO_4)_3 \cdot 8H_2O$ for SK, a new process has been developed. It utilizes the difference of precipitation pH between gadolinium hydroxide and radium hydroxide. By adding a base to an acidic aqueous solution of the raw material and adjusting the pH of the aqueous solution between 8 and 9, gadolinium precipitates as gadolinium hydroxide while maintaining the state in which radium is still dissolved in the aqueous phase. As bases for pH adjustment, ammonia, sodium hydroxide, and potassium hydroxide can be considered. It is highly preferable to use ammonia for pH adjustment to avoid contamination with other metals such as sodium or potassium. During a test, 25% by mass aqueous ammonia was gradually added to the aqueous gadolinium chloride solution after dissolving gadolinium oxide to adjust the pH to 8.0. Gadolinium hydroxide can then be obtained as a precipitate. The amount of ammonia water added to 10 kg of the gadolinium chloride solution was 4.7 kg. The precipitate was separated by filtration and washed with water until the chloride ion concentration of the filtrate became 1000 mg/L or less to obtain gadolinium hydroxide. The obtained hydroxide is again dissolved in 35% by mass hydrochloric acid aqueous solution to obtain an acidic aqueous gadolinium solution which is an input to the solvent extraction. As shown in Table 7, we succeeded in reducing radium to less than 1% of its previous value with this new process.

8. Conclusions

This paper reports the development and detailed properties of about 13 metric tons of $Gd_2(SO_4)_3 \cdot 8H_2O$ which has been dissolved into SK in the summer of 2020. We evaluated the impact of radioactive impurities in $Gd_2(SO_4)_3 \cdot 8H_2O$ on DSNB searches and solar neutrino observations. We confirmed the need to reduce radioactive and fluorescent impurities by about three orders of magnitude from commercially available high-purity $Gd_2(SO_4)_3 \cdot 8H_2O$. Therefore, we developed a method to remove impurities from Gd_2O_3 by acid dissolution, solvent extraction, and pH control processes, and then we developed a high-purity sulfation pro-

cess. All of the produced high-purity $Gd_2(SO_4)_3 \cdot 8H_2O$ batches were sampled and assayed by ICP-MS and HPGe detectors to evaluate their quality. Because the HPGe assays require long measurement times to achieve sufficient sensitivity to distinguish very low levels of radioactive impurities, measurements were performed in cooperation with HPGe detectors at LSC in Spain, Boulby in the UK, and Kamioka in Japan.

In the first half of production, the assayed batch purities were consistent with the specifications. However, it was found that the $Gd_2(SO_4)_3 \cdot 8H_2O$ in the latter half of the produced batches contained one order of magnitude more ^{228}Ra than the budgeted mean contamination. This was correlated with the corresponding characteristics of the raw material Gd_2O_3, in which an intrinsically large contamination was present and could not affordably be replaced with raw material of ideal condition. However, since the increase of the background event rate for solar neutrino observations due to this activity of ^{228}Ra is at the same level as the background in the pure water phase of SK, the decision was made to introduce these later batches into SK anyway.

A new method to remove ^{228}Ra from Gd_2O_3 has been subsequently established. Introduced into SK in 2022, the latest 26 metric tons of $Gd_2(SO_4)_3 \cdot 8H_2O$ show the required high purity.

Acknowledgments

We gratefully acknowledge the Super-Kamiokande experiment. It has been built and operated from funding by the Japanese Ministry of Education, Culture, Sports, Science and Technology, the US Department of Energy, and the US National Science Foundation. We also acknowledge the cooperation of the Kamioka Mining and Smelting Company, Japan. Some of us have been supported by funds from the Ministry of Education, Japan, 2018R1D1A3B07050696, 2018R1D1A1B07049158, the Japan Society for the Promotion of Science (JSPS) KAKENHI Grants Grant-in-Aid for Scientific Research on Innovative Areas No. 26104004, 26104006, 17H06365, 19H05807, 19H05808, Grant-in-Aid for Specially Promoted Research No. 26000003, Grant-in-Aid for Young Scientists No. 17K14290, and Grant-in-Aid for JSPS Research Fellow No. 18J00049, Universities and Innovation grant PID2021-124050NB-C31, the European Union's Horizon 2020 Research and Innovation Programme under the Marie Sklodowska-Curie 2020-MSCA-RISE-2019 SK2HK grant agreement no. 872549. We acknowledge Israel Chemicals Ltd UK (ICL-UK) for hosting the UK Science and Technology Facilities Council's (STFC) Boulby Underground Laboratory. The authors from Sheffield were supported by the STFC under award nos. ST/R000069/1, ST/T00200X/1, ST/V002821/1, ST/V006185/1, and ST/S000747/1. We are grateful to the Laboratorio Subterráneo de Canfranc (Spain) for supporting the low-background materials screening work.

Appendix A. X-ray diffraction analysis

An example of X-ray diffraction data of one batch sample is shown in Fig. A1. Since $Gd_2(SO_4)_3 \cdot 8H_2O$ particles have high crystallinity, the orientation dependence of each peak intensity is high. Therefore, the intensity may change depending on how it is packed in a holder, so the peak positions (not the relative intensities) must be checked. As a result, all the peak positions are in agreement with the X-ray diffraction database: ICPDS # 01-81-1794: gadolinium sulfate octahydrate.

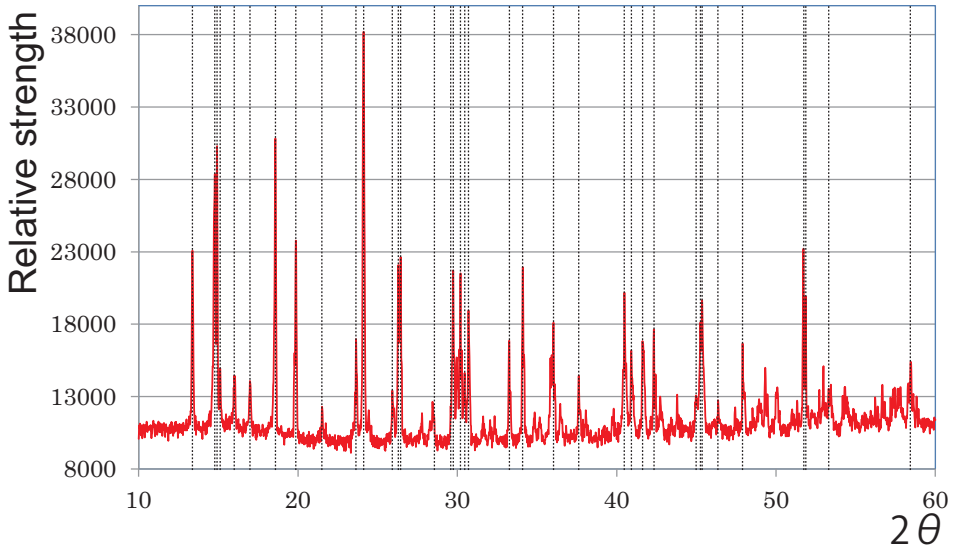

Figure A1. Example of X-ray diffraction data (red); peak positions in the ICPDS database (# 01-81-1794: gadolinium sulfate octahydrate) are shown as dashed lines (black).

Appendix B. Thermogravimetric analysis

An example of thermogravimetric analysis data of one batch sample is shown in Fig. B1. The sample is heated from room temperature to 800°C, and the mass change with temperature is measured. Figure B1 shows the mass loss and the heat flow as functions of sample temperature. The mass loss observed near 100°C is mainly due to the evaporation of the water remaining during purification, and the mass loss at higher temperatures is due to the evaporation of the octahydrate from $Gd_2(SO_4)_3 \cdot 8H_2O$. The expected mass loss due to going from an octahydrate to an anhydrous form of gadolinium sulfate is 19.3%.

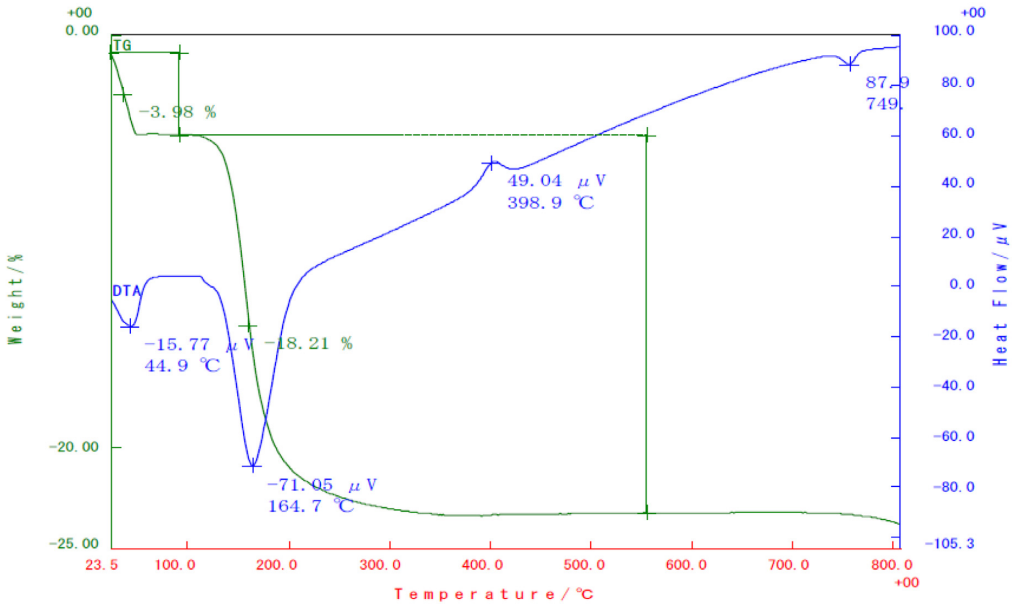

Figure B1. Mass loss and C.heat flow as functions of sample temperature.

References

[1] Y. Fukuda et al., Nucl. Instrum. Meth. A **501**, 418 (2003).
[2] J. F. Beacom and M. R. Vagins, Phys. Rev. Lett. **93**, 171101 (2004), hep-ph/0309300.
[3] K. Abe et al., Nucl. Instrum. Meth. A **1027**, 166248 (2022), [arXiv:2109.00360] [Search inSPIRE].
[4] A. G. Popeko and G. M. Ter-Akopian, Nucl. Instrum. Meth. **178**, 163 (1980).
[5] H. W. Sobel, A. A. Hruschka, W. R. Kropp, J. Lathrop, F. Reines, M. F. Crouch, B. S. Meyer, and J. P. F. Sellschop, Phys. Rev. C **7**, 1564 (1973).
[6] A. G. Popeko, V. I. Smirnov, G. M. Ter-Akop'yan, B. V. Fefilov, and L. P. Chelnokov, Sov. J. Nucl. Phys. (Engl. Transl.), (United States) **24**:3 (1976).
[7] T. Ethvignot, M. Devlin, H. Duarte, T. Granier, R. C. Haight, B. Morillon, B. R. O. Nelson, J. M. O'Donnell, and D. Rochman, Phys. Rev. Lett. **94**, 052701 (2005).
[8] P. Fernández Menéndez, Neutrino physics in present and future Kamioka water-Cherenkov detectors with neutron tagging, PhD thesis, Universidad Autonoma, Madrid (2017).
[9] K. Abe et al., Phys. Rev. D **104**, 122002 (2021).
[10] K. Abe et al., Phys. Rev. D **94**, 052010 (2016).
[11] W. B. Wilson, R. T. Perry, E. F. Shores, W. S. Charlton, T. A. Parish, G. P. Estes, T. H. Brown, E. D. Arthur, M. Bozoian, T. R. England, D. G. Madland, and J. E. Stewart, SOURCES 4C : a code for calculating ([alpha],n), spontaneous fission, and delayed neutron sources and spectra, (2002), https://www.osti.gov/biblio/976142.
[12] T. Shigematsu, Y. Nishikawa, K. Hiraki, S. Goda, and Y. Tsujimoto, Bunseki Kagaku **20**(5), 575 (1971).
[13] Ll. Marti et al., Nucl. Instrum. Meth. A **959**, 163549 (2020), [arXiv:1908.11532] [Search inSPIRE].
[14] K. Abe et al., Nucl. Instrum. Meth. Phys. Res. A **1027**, 166248 (2022).
[15] A. Kumari, R. Panda, M. K. Jha, and D. D. Pathak, Comptes Rendus Chimie **21**, 1029 (2018).
[16] P. R. Scovell et al., Astropart. Phys. **97**, 160 (2018).
[17] D. S. Akerib et al., Eur. Phys. J. **C80**, 1 (2020).
[18] S. Agostinelli et al., Nucl. Instrum. Meth. Phys. Res. A **506**, 250 (2003).
[19] M. Thiesse, P. Scovell, and L. Thompson, Appl. Radiat. Isot. **188**, 110384 (2022).
[20] Mirion Technologies (Canberra) France SAS , https://www.mirion.com/ (data last accessed 2021-12-20).
[21] K. Abe et al., J. Instrum. **15**(09), P09027 (2020).
[22] S. Ito et al., Prog. Theor. Exp. Phys. **2018**, 091H01 (2018).
[23] S. Ito et al., Prog. Theor. Exp. Phys. **2020**, 093H02 (2020).
[24] C. Hurtgen, S. Jerome, and M. Woods, Appl. Radiat. Isot. **53**, 45 (2000).